

# Source-size measurements and charge distributions of ions accelerated from thin foils irradiated by high-intensity laser pulses

J. SCHREIBER<sup>1,2,✉</sup>  
M. KALUZA<sup>1</sup>  
F. GRÜNER<sup>2</sup>  
U. SCHRAMM<sup>2</sup>  
B.M. HEGELICH<sup>3</sup>  
J. COBBLE<sup>3</sup>  
M. GEISSLER<sup>1</sup>  
E. BRAMBRINK<sup>4</sup>  
J. FUCHS<sup>5,6</sup>  
P. AUDEBERT<sup>5</sup>  
D. HABS<sup>2</sup>  
K. WITTE<sup>1</sup>

<sup>1</sup> MPI für Quantenoptik, Hans-Kopfermann-Str. 1, 85748 Garching, Germany  
<sup>2</sup> LMU München, Am Coulombwall 1, 85748 Garching, Germany  
<sup>3</sup> Los Alamos Natl. Lab, P.O. Box 1663 Los Alamos, NM 87545, USA  
<sup>4</sup> TU Darmstadt, Schloßgartenstr. 9, 64289 Darmstadt, Germany  
<sup>5</sup> Laboratoire pour l'Utilisation des Lasers Intenses, UMR 7605 CNRS-CEA-École Polytechnique-Univ. Paris VI, Palaiseau, France  
<sup>6</sup> Physics Department, MS-220, University of Nevada, Reno, Nevada 89557, USA

Received: 16 June 2004/Revised version: 8 September 2004  
Published online: 26 October 2004 • © Springer-Verlag 2004

**ABSTRACT** We report on measurements of source sizes and charge state distributions of ions accelerated from thin foils irradiated by ultrashort (100–300 fs) high-intensity ( $1 - 6 \times 10^{19}$  W/cm<sup>2</sup>) laser pulses. The source sizes of proton and carbon ion beams originating from hydrocarbon contaminants on the surfaces of 5  $\mu$ m thick aluminum foils were investigated using the knife-edge method. For low-energy protons and low-carbon charge states, the source area was found to exceed the focal spot area by a factor of  $10^4$ . For the determination of charge state distributions, sandwich targets consisting of a 25  $\mu$ m thick tungsten layer, a 2-nm thin beryllium layer, and again a tungsten layer whose thickness was varied were used. These targets were resistively heated to remove the light surface contaminants. Peaked energy spectra of oxygen and argon ions corresponding to the equilibrium distribution after propagation through matter were observed.

**PACS** 41.75.Jv; 52.38.Kd; 52.25.Jm; 52.50.Jm; 52.70.Nc; 41.75.Ak

## 1 Introduction

The effective acceleration of ions by ultrashort (30 fs–1 ps) high-intensity ( $10^{18}$ – $10^{21}$  W/cm<sup>2</sup>) laser pulses interacting with thin foils attracted high attention during recent years. The emitted ion and, in particular, proton pulses reached large particle numbers between  $10^{10}$  and  $10^{13}$  with energies in the MeV- [1, 2] and multi-MeV-range [3–6]. In recent experiments, the high quality of proton beams emitted from the rear side of laser irradiated thin foils was proved [7–9]. On this account, they have been considered as an ion source for the injection into a conventional particle accelerator [10] and for fast ignition [11]. Moreover, laser-accelerated protons were successfully used for diagnosing the electromagnetic fields in overdense laser-produced plasmas with a picosecond time resolution soon after they were first observed [12]. The potential of using protons as an indirect

diagnostic for the electron transport through solid targets has also been demonstrated [13].

The acceleration of ions during the laser-plasma interaction is qualitatively understood. When a laser pulse of relativistic intensity ( $I\lambda^2 > 10^{18}$  W/cm<sup>2</sup>  $\times$   $\mu$ m<sup>2</sup>) impinges on a solid surface or a preformed plasma, electrons are accelerated to relativistic velocities within half an oscillation period (1–2 fs for typical laser wavelengths). Simultaneously, they are bent into the propagation direction of the laser pulse because of the  $\mathbf{v} \times \mathbf{B}$ -term in the Lorentz-force referred to as ponderomotive potential when cycle-averaged. There are additional mechanisms for energy absorption in presence of steep density gradients ([14] and references therein) which will not be discussed here. However, the ions remain at rest since they are too massive to follow the fast laser oscillation. Thus a quasi-stationary electric field is formed near the critical density surface due to this laser driven charge separation. This is most likely the source of the front-side accelerated ions observed in various experiments [15]. The fastest electrons ( $\sim$  MeV mean energy) travel through the foil and escape on their rear-side leaving a charged target behind. With increasing quasi-static electrical potential, slower electrons are no longer able to leave the target. They form a  $\mu$ m-scale Debye-sheath at the target rear side, where the electric field reaches values in the TV/m-regime. Atoms on the target rear-side experience field ionization and are subsequently accelerated. Emerging from this sheath region, the ions gain kinetic energies of several MeV per nucleon [4, 6, 16]. As the electric field points normal to the target surface, this process is called target normal sheath acceleration (TNSA) [17]. For the laser parameter range and target properties this paper deals with, it has been shown that TNSA is dominant over front-side-acceleration [18, 19].

A series of experiments was performed to investigate the dependence of the observed ion spectra on the intensity [14, 20] and contrast ratio [2, 21] of the laser pulse as well as on different target properties [2, 4, 21]. Although some theories exist reproducing experimental data [22, 23], none of them includes all physically relevant processes. Since in most experiments hydrocarbons contaminated the target surfaces, protons got accelerated predominantly due to their high

✉ Fax: +49-89-32905-200, E-mail: joerg.schreiber@mpq.mpg.de

charge-to-mass ratio and thus were the subject of the most studies. Nevertheless, carbon and even heavier ions of various charge states are usually observed simultaneously under these conditions, albeit with lower number and energy [16, 20, 24]. However, neither the appearance of the observed charge state distributions nor their spatial origin in terms of source size and shape can be explained by the models so far. For the latter, some experimental estimates were already obtained showing that the source size of the rear-side accelerated protons is much larger than the laser focal spot [4, 7–9]. In all these experiments protons were studied. Their number usually exceeds the number of heavier ions by a factor of 100 or more. Additionally, stacks of radiochromic film were used as an ion-detector. These stacks are usually shielded with an aluminum foil, which stops the heavier ions. For a simultaneous source-size measurement of protons and, e.g., carbon ions, the different species and charge states must be separated. In a single shot experiment, this can be done with a Thomson parabola spectrometer only.

A rather simple experiment for source size measurements of protons and carbon ions will be described in Sect. 2 using the knife-edge method. Sect. 3 will address an experiment where oxygen and argon ions could be accelerated. This could be achieved by heating the target to temperatures exceeding 1000 °C. Although it is not yet clear if a major fraction of the contaminant elements is removed or if it diffuses into the target, this technique is appropriate for heavy ion acceleration as demonstrated in [16, 24].

## 2 Source size measurements

The experiments were performed at the ATLAS10 10-Hz-tabletop-laser-system at the MPQ Garching providing laser pulses with energies of about 0.75 J and 150-fs full width at half maximum (FWHM) duration at a center wavelength of 790 nm. Single laser pulses were focused onto 5- $\mu\text{m}$  thick aluminum foils with an incident angle of 30° reaching an intensity of  $2 \times 10^{19} \text{ W/cm}^2$  in a spot of 3- $\mu\text{m}$  FWHM diameter. The duration of the amplified spontaneous emission (ASE) was controlled by a fast Pockels cell and chosen to be 1 ns with an intensity contrast of better than  $2 \times 10^7$ . This pedestal generated a pre-plasma with a scale length of 4  $\mu\text{m}$  at the critical density. Ion spectra were recorded in the target normal direction ( $\pm 5$  mrad) using a Thomson parabola spectrometer with a pinhole of 300- $\mu\text{m}$  diameter placed 80 cm behind the target (Fig. 1). Nuclear track detectors (CR39) were used inside the Thomson parabola spectrometer to record the ion tracks. After etching, the ion pits were counted by a commercial automated scanning system composed of a computer-controlled optical microscope and a pattern recognition software. This standard experimental setup was extended by the introduction of a scraper placed 8 mm behind the target to perform the knife-edge measurements by moving the scraper across the beam. A stainless steel razor-blade served for this purpose. Since the solid angle of the ion beam ( $\sim 25$  msr) was about 5 orders of magnitude larger than the detector solid angle (area of entrance aperture of the Thomson parabola spectrometer/(distance to target)<sup>2</sup>,  $10^{-4}$  msr), only a small fraction of the signal passing the scraper was detected (Fig. 1). This is important for the interpretation of the results.

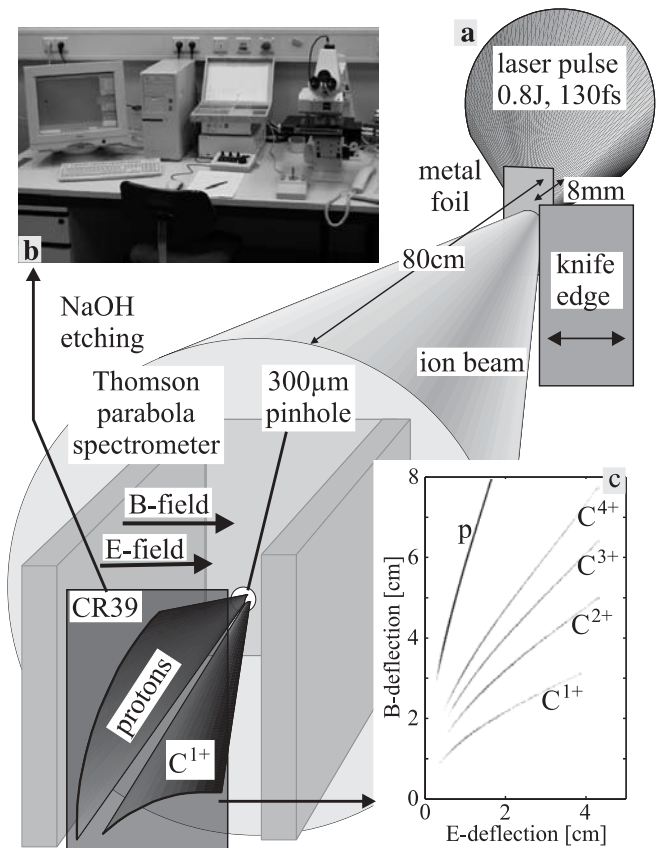


**FIGURE 1** Experimental setup. (a) The laser pulse is focused by an off-axis parabola onto the foil target with an incident angle of 30°. The ions are detected in target normal direction with a Thomson parabola type spectrometer using CR39 plastic track detectors. After irradiation they are etched in sodium leauge and scanned by a computer controlled microscope (b). Every single ion track is counted leading to a density image (c) from which the spectra are calculated

Figure 2 shows the spectra of protons and carbon ions with charge states 1+ to 4+ for six selected scraper positions, namely with the scraper at the center of the ion beam (a) and successively moved inwards in 40  $\mu\text{m}$ -steps (b–f). For the next scraper position, following (f) corresponding to 240  $\mu\text{m}$  off center, no ions are detected. The high-energy protons ( $E_{\text{kin}} > 0.8$  MeV) and highly charged carbon ions ( $\text{C}^{4+}$ ,  $E_{\text{kin}} > 2.5$  MeV) already vanish after the first scraper step (40  $\mu\text{m}$ ) whereas the low-energy protons ( $< 0.8$  MeV) and the lower carbon charge states appear to be unaffected. The maximum kinetic energy both of protons and  $\text{C}^{4+}$ -ions decreases with the scraper sliding into the ion beam. Only protons and singly-charged carbon ions remain at the last scraper position (Fig. 2f). The deflection of the ions with the lowest energies was calculated assuming that the scraper is charged with 1 nC. This is a reasonable value for the charge carried by the fast electrons leaving the target. The deflection in the plane of the Thomson parabola spectrometer pinhole was 40  $\mu\text{m}$  and 100  $\mu\text{m}$  for protons and  $\text{C}^{4+}$ -ions, respectively. Since the pinhole diameter was 300  $\mu\text{m}$ , the influence of the scraper on the passing ions was neglected.

The appearance of only singly ionized carbon in the outer regions indicates a radial decrease in the strength of the quasi-static electric field. As it was discussed in [16], field ionization

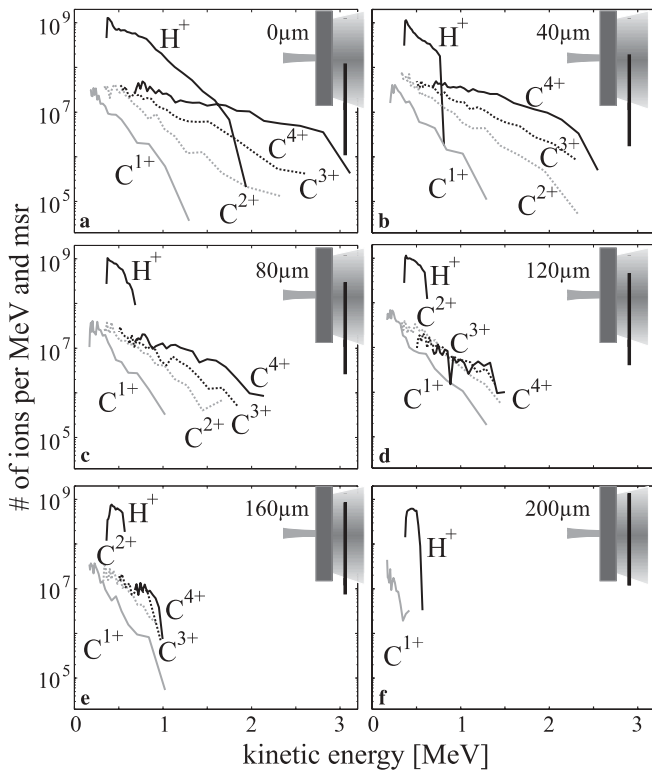


**FIGURE 2** Proton and ion spectra for different scraper positions, starting from the center (a)

is the dominant ionization mechanism. In this case, a significant number of ions with a certain charge state can be produced only in regions where the field once exceeded the respective threshold. It thus depicts a lower boundary for the field in this place. The appearance of a maximum ion charge state suggests that the field was never larger than the threshold for the ionization to the next charge state thus giving an upper bound. Although the latter statement implies that no charge exchange occurs after the field ionization process, these assumptions have been used to derive the radial field profile. By reading out the ion spectra of Fig. 2 one can estimate the max-

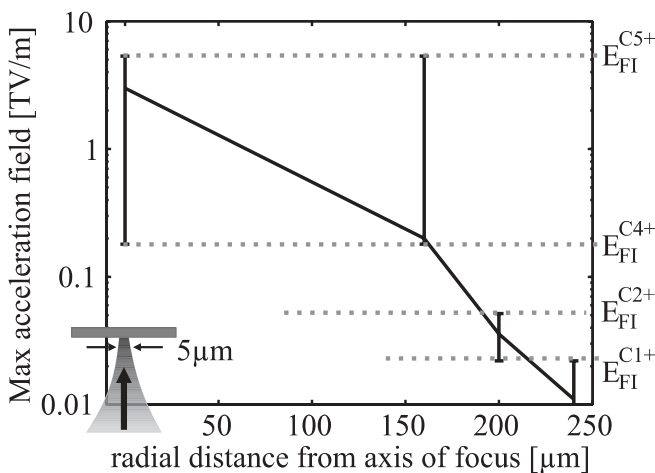


**FIGURE 3** Radial profile of the maximum field present during the acceleration process. The error bars represent the threshold fields for field ionization (FI)

imal field which was present during the acceleration process (Fig. 3). The field strength in the center of the emission area was estimated using the formula  $E = \sqrt{2/e \times n_{e0} k_b T_e / \epsilon_0}$  [25] where  $\epsilon_0$  is the vacuum dielectric constant and  $e$  is Euler's constant. The product of the mean energy ( $k_b T_e$ ) and the density of the fast electrons ( $n_{e0}$ ) can be expressed by  $n_{e0} k_b T_e = \eta \cdot I/c$ , where  $I$  is the laser intensity,  $c$  is the velocity of light, and  $\eta$  is the conversion ratio of laser energy into hot electrons chosen to be 10 percent.

Due to the small solid angle of the Thomson parabola spectrometer ( $10^{-4}$  msr) as compared to the opening angle of the emitted ion beam ( $\sim 25$  msr), the knife-edge method can not be used for the complete characterization of the source. In recent experiments [8], it was shown that the proton beams emitted from the rear side of thin foils exhibit a small normalized emittance ( $< 0.004 \pi \text{mm} \times \text{mrad}$ ). Moreover, their angular divergence depends linearly on the radial distance to the laser focal spot for the considered proton energies. If these results apply to the present case, the ion signal should vanish as soon as the scraper passes the center of the emitting area. In fact this is what happens for the high-energy protons and  $C^{4+}$ -ions (Fig. 2a–b). Nevertheless this principle does not seem to apply to the low-energy protons and carbon ions. They might have a larger emittance or emit more straight than the high-energy ions, so ions stemming from the outer areas are able to hit the pinhole of the spectrometer. This could also be caused by a bumpy sheath, where different spatial zones emit ions in target-normal direction. To find a lower constraint for the measured source sizes, it appears most feasible to assume that the ions stem from a circular source, where every point was considered to make the same contribution to the spectrometer signal. For this case, the measured signal can be written as  $S = N_0/2 \left[ 1 - 2/\pi \left( \sin^{-1} x_n + x_n \sqrt{1 - x_n^2} \right) \right]$ , where  $N_0$  is the number of ions in a certain energy interval observed without using the scraper and  $x_n = 2x_s/s$  is the scraper position  $x_s$  divided by the energy-dependent source size  $s$ , which is the fit parameter. Figure 4 shows the calculated source sizes of

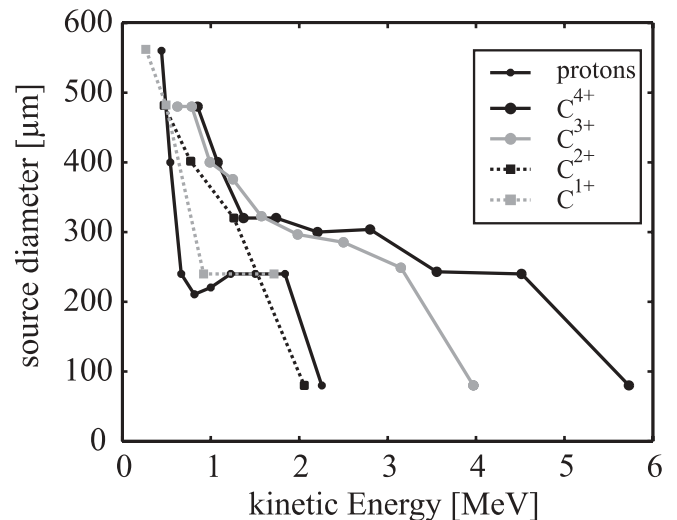


**FIGURE 4** Proton and ion source sizes versus kinetic energy. The values represent lower limits for the source diameters

protons and carbon ions as a function of their kinetic energy resulting from the above model assumptions. The denoted values represent a lower boundary for the source diameters except for the high-energy ions. They are confined by the smallest detectable diameter of  $80\ \mu\text{m}$ , which is twice as high as the scraper step width.

The heavier ions, e.g. carbon, represent only a minor fraction of the total number of ions in experiments using hydrocarbon-contaminated metal targets. This picture changes dramatically once the targets are heated. In this case, protons can be completely removed from the target surfaces resulting in a much larger number and energy of the heavy ions. The next section addresses measurements of charge state distributions of ions accelerated from heated sandwich-targets.

### 3 Heavy ion measurements – heated targets

In most experiments, hydrocarbon and water contaminants cover the target surface. Here we describe experiments employing resistive heating to remove these contaminants [16]. The 100-TW laser system at the Laboratoire pour l'Utilisation des Lasers Intenses (LULI) at École Polytechnique was used for this campaign. It delivers pulses with an energy of 20 J and a FWHM duration of 320 fs in a focal spot of  $6\text{-}\mu\text{m}$  FWHM diameter reaching an intensity of  $6 \times 10^{19}\ \text{W}/\text{cm}^2$ . Except for the fact that the laser was normally incident and the scraper was removed, the experimental setup was similar to that depicted in Fig. 1. Instead of the aluminum, we used tungsten foils ( $25\ \mu\text{m}$ ) the rear-sides of which were coated with a thin ( $\sim 2\ \text{nm}$ ) beryllium layer followed by a layer of tungsten of variable thicknesses (0–40 nm). This target geometry was chosen aiming at a measurement of the depth profile of the rear-side acceleration field inside the foil by measuring the number of beryllium ions as a function of the tungsten layer thickness. This topic will be discussed in more detail elsewhere. To our surprise, we found oxygen ions from the first up to the sixth charge state in each shot. Since no protons or carbon ions were observed, the oxygen ions most probably originate from oxide layers of the tungsten rather than from water contaminants. Tungsten accumulates an oxide layer similar to aluminum. Furthermore, the  $25\ \mu\text{m}$ -tungsten foil was milled under red heat ( $\sim 800\ ^\circ\text{C}$ ) resulting in an oxide-layer buried under the beryllium-tungsten-sandwich structure. Additionally, argon ions ( $1+$  to  $8+$ ) were present in some of the shots. This is not surprising since they were used as sputtering projectiles for the target coating process. Usually a small fraction of these ions incorporate into the sputtered layers. The  $\text{O}^{6+}$ -ions with maximum kinetic energies of  $2\ \text{MeV}/\text{u}$  were the most energetic species measured. Typical spectra of oxygen and argon ions taken from one shot where both species were present are shown in Fig. 5a and b separately.

The total ion spectra were calculated by adding the spectral distributions of the different charge states for both elements. The spectra can be described by double exponential distributions with mean energies of  $62\ \text{keV}/\text{u}$  and  $0.4\ \text{MeV}/\text{u}$  for oxygen and  $17\ \text{keV}/\text{u}$  and  $0.1\ \text{MeV}/\text{u}$  for argon (Insets of Fig. 5a,b). The spectra of the individual charge states are shifted to higher energies with increasing charge. Note the

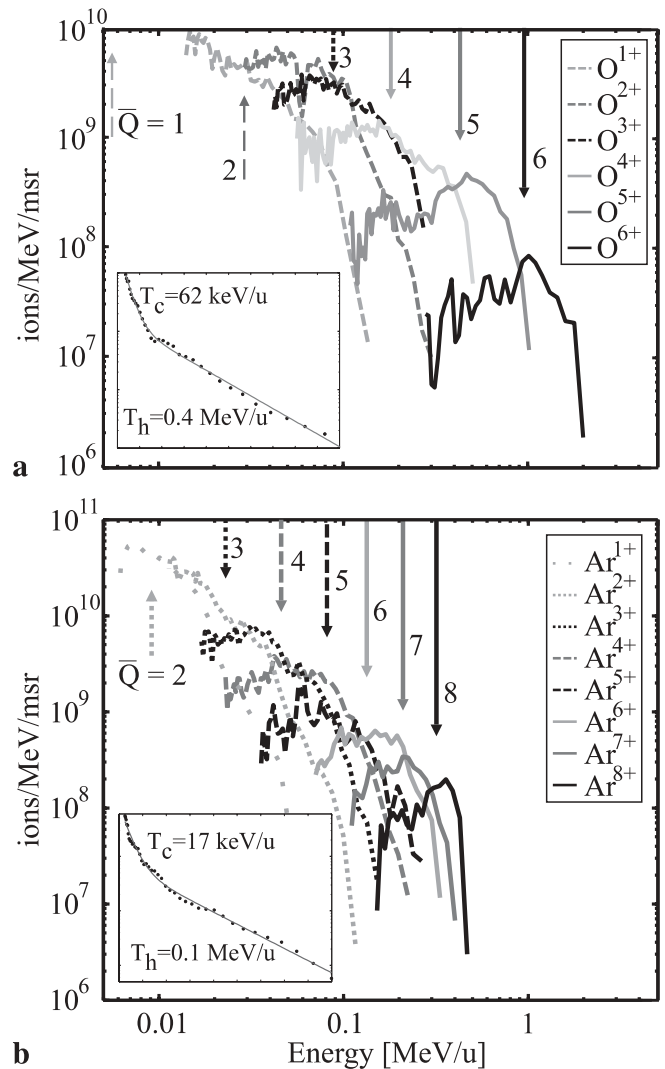


**FIGURE 5** Spectra of oxygen (a) and argon (b) ions from an irradiated  $25\text{-}\mu\text{m}$  tungsten/2-nm beryllium sandwich-target. The arrows depict the kinetic energy an ion needs to reach the given charge states in case of charge equilibrium. The total spectra of the oxygen and argon ions are shown in the insets. The spectra can be fitted by a double exponential function with mean energies,  $T_c$  and  $T_h$

pronounced maxima appearing in the spectral distributions, especially for the higher charge states. The arrows depict the kinetic energies at which the corresponding ions, in case of charge equilibrium, take on the given charge states in solids. The values for  $\text{O}^{4+}$  to  $\text{O}^{6+}$  were taken from measured equilibrium charge states for oxygen ions after having passed through gold foils [26], which is close to tungsten. Since experimental data are lacking, the respective values for argon and the lower oxygen equilibrium charge states were calculated using the empirical formula given in [27]. The observed maxima are close to the equilibrium charge states. This finding basically means that the detected ions must have left the foil with their final energy and the corresponding charge state. Taking into account that these ions started at rest, a considerable acceleration distance inside the foil is required. This gives two possibilities for their original locations, because the rear-surface is ruled out as ions originating from there lack sufficient matter to reach charge state equilibrium by electron

exchange reactions. The front-side appears possible, however, oxygen ions need about 100 MeV to traverse 25  $\mu\text{m}$  of tungsten. Therefore, we tentatively propose that the observed oxygen and argon ions came from the bulk of the foil, at least from a thick enough region underneath the rear-surface.

#### 4 Conclusion

Experiments using the knife-edge method were performed to determine the source extension of protons and carbon ions accelerated from thin aluminum foils irradiated with high-intensity laser pulses. The quasi-static electric field was reduced by two orders of magnitude within a radial distance of 200  $\mu\text{m}$  from the laser focus. The source extension of the most energetic protons ( $> 0.8$  MeV) was smaller than 80  $\mu\text{m}$  which is in good agreement with earlier proton source size measurements [4, 8, 9]. Moreover, it was shown that the most energetic  $\text{C}^{4+}$ -ions ( $> 2.5$  MeV) originate from the same central spot. Source size diameter up to 500  $\mu\text{m}$  were observed for the low energy protons and carbon ions.

In the second experiment oxygen and argon ions emitted from coated tungsten foils were observed. The targets were resistively heated to remove the hydrocarbon and water contaminant layers. The total spectra could be described by double exponential distributions, whereas the individual charge state spectra overlapped and were shifted to higher energies with higher charge states. The observed pronounced maxima were compared to equilibrium charge state distributions well known from stripper-foil experiments in accelerator physics [26, 27]. For the found agreement we have suggested an explanation in terms of starting positions of the detected ions underneath the rear-surface.

**ACKNOWLEDGEMENTS** This work was supported by grant E1127 from Région Ile-de-France, and UNR grant DE-FC08-01NV14050 as well as DFG HA 1101/7, GSI LM-HA3 and BMBF 06ML184.

#### REFERENCES

- 1 A.P. Fews, P.A. Norreys, F.N. Beg, A.R. Bell, A.E. Dangor, C.N. Danson, P. Lee, S.J. Rose: *Phys. Rev. Lett.* **73**, 1801 (1994)
- 2 A. Maksimchuk, S. Gu, K. Flippo, D. Umstadter, V.Yu. Bychenkov: *Phys. Rev. Lett.* **84**, 4108 (2000)
- 3 E.L. Clark, K. Krushelnick, J.R. Davies, M. Zepf, M. Tatarakis, F.N. Beg, A. Machacek, P.A. Norreys, M.I.K. Santala, I. Watts, A.E. Dangor: *Phys. Rev. Lett.* **84**, 670 (2000)
- 4 R.A. Snavely, M.H. Key, S.P. Hatchett, T.E. Cowan, M. Roth, T.W. Phillips, M.A. Stoyer, E.A. Henry, T.C. Sangster, M.S. Singh, S.C. Wilks, A. MacKinnon, A. Offenberger, D.M. Pennington, K. Yasuike, A.B. Langdon, B.F. Lasinski, J. Johnson, M.D. Perry, E.M. Campbell: *Phys. Rev. Lett.* **85**, 2945 (2000)
- 5 S.P. Hatchett, C.G. Brown, T.E. Cowan, E.A. Henry, J.S. Johnson, M.H. Key, J.A. Koch, A.B. Langdon, B.F. Lasinski, R.W. Lee, A.J. Mackinnon, D.M. Pennington, M.D. Perry, T.W. Phillips, M. Roth, T.C. Sangster, M.S. Singh, R.A. Snavely, M.A. Stoyer, S.C. Wilks, K. Yasuike: *Phys. Plasmas* **7**, 2076 (2000)
- 6 A.J. Mackinnon, M. Borghesi, S. Hatchett, M.H. Key, P.K. Patel, H. Campbell, A. Schiavi, R. Snavely, S.C. Wilks, O. Willi: *Phys. Rev. Lett.* **86**, 1768 (2001)
- 7 M. Roth, M. Allen, P. Audebert, A. Blazevic, E. Brambrink, T.E. Cowan, J. Fuchs, J.-C. Gauthier, M. Geißel, M. Hegelich, S. Karsch, J. Meyer-ter-Vehn, H. Ruhl, T. Schlegel, R.B. Stephens: *Plasma Phys. Control. Fusion B* **44**, 99 (2002)
- 8 T.E. Cowan, J. Fuchs, H. Ruhl, A. Kemp, P. Audebert, M. Roth, R. Stephens, I. Barton, A. Blazevic, E. Brambrink, J. Cobble, J. Fernández, J.-C. Gauthier, M. Geißel, M. Hegelich, J. Kaae, S. Karsch, G.P. Le Sage, S. Letzring, M. Manclossi, S. Meyroneinc, A. Newkirk, H. Pépin, N. Renard-LeGalloudec: *Phys. Rev. Lett.* **92**, 204801 (2004)
- 9 M. Borghesi, A.J. Mackinnon, D.H. Campbell, D.G. Hicks, S. Kar, P.K. Patel, D. Price, L. Romagnani, A. Schiavi, O. Willi: *Phys. Rev. Lett.* **92**, 055003 (2004)
- 10 H. Haseroth, H. Hora: *Laser & particle beams* **14**, 393 (1996)
- 11 M. Roth, T.E. Cowan, M.H. Key, S.P. Hatchett, C. Brown, W. Fountain, J. Johnson, D.M. Pennington, R.A. Snavely, S.C. Wilks, K. Yasuike, H. Ruhl, F. Pegoraro, S.V. Bulanov, E.M. Campbell, M.D. Perry, H. Powell: *Phys. Rev. Lett.* **86**, 436 (2001)
- 12 M. Borghesi, S. Bulanov, D.H. Campbell, R.J. Clark, T.Zh. Esirkepov, M. Galimberti, L.A. Gizzi, A.J. MacKinnon, N.M. Naumova, F. Pegoraro, H. Ruhl, A. Schiavi, O. Willi: *Phys. Rev. Lett.* **88**, 135002 (2002)
- 13 J. Fuchs, T.E. Cowan, P. Audebert, H. Ruhl, L. Gremillet, A. Kemp, M. Allen, A. Blazevic, J.C. Gauthier, M. Geißel, M. Hegelich, S. Karsch, P. Parks, M. Roth, Y. Sentoku, R. Stephens, E.M. Campbell: *Phys. Rev. Lett.* **91**, 255002 (2003)
- 14 F.N. Beg, A.R. Bell, A.E. Dangor, C.N. Danson, A.P. Fews, M.E. Glinzsky, B.A. Hammel, P. Lee, P.A. Norreys, M. Tatarakis: *Phys. Plasmas* **4**, 447 (1997)
- 15 K. Nemoto, A. Maksimchuk, S. Banerjee, K. Flippo, G. Mourou, D. Umstadter, V.Yu. Bychenkov: *Appl. Phys. Lett.* **78**, 595 (2001)
- 16 M. Hegelich, S. Karsch, G. Pretzler, D. Habs, K. Witte, W. Guenther, M. Allen, A. Blazevic, J. Fuchs, J.-C. Gauthier, M. Geißel, P. Audebert, T.E. Cowan, M. Roth: *Phys. Rev. Lett.* **89**, 085002 (2002)
- 17 S.C. Wilks, A.B. Langdon, T.E. Cowan, M. Roth, M. Singh, S. Hatchett, M.H. Key, D. Pennington, A. MacKinnon, R.A. Snavely: *Phys. Plasmas* **8**, 542 (2001)
- 18 S. Karsch, S. Düsterer, H. Schwoerer, F. Ewald, D. Habs, M. Hegelich, G. Pretzler, A. Pukhov, K. Witte, R. Sauerbrey: *Phys. Rev. Lett.* **91**, 015001 (2003)
- 19 J. Fuchs, Y. Sentoku, S. Karsch, J. Cobble, P. Audebert, A. Kemp, A. Nikroo, P. Antici, E. Brambrink, A. Blazevic, E.M. Campbell, J.C. Fernández, J.-C. Gauthier, M. Geißel, M. Hegelich, H. Pépin, H. Popescu, N. Renard-LeGalloudec, M. Roth, J. Schreiber, R. Stephens, T.E. Cowan: submitted to *Phys. Rev. Lett.*
- 20 E.L. Clark, K. Krushelnick, M. Zepf, F.N. Beg, M. Tatarakis, A. Machacek, M.I.K. Santala, I. Watts, P.A. Norreys, A.E. Dangor: *Phys. Rev. Lett.* **85**, 1654 (2000)
- 21 M. Kaluza, J. Schreiber, M.I.K. Santala, G.D. Tsakiris, K. Eidmann, J. Meyer-ter-Vehn, K.J. Witte: *Phys. Rev. Lett.* **93**, 045003 (2004)
- 22 A. Pukhov: *Phys. Rev. Lett.* **86**, 3562 (2001)
- 23 P. Mora: *Phys. Rev. Lett.* **90**, 185002 (2003)
- 24 M. Zepf, E.L. Clark, F.N. Beg, R.J. Clarke, A.E. Dangor, A. Gopal, K. Krushelnick, P.A. Norreys, M. Tatarakis, U. Wagner, M.S. Wei: *Phys. Rev. Lett.* **90**, 064801 (2003)
- 25 J.E. Crow, P. L. Auer, J.E. Allen: *J. Plasma Phys.* **14**, 65 (1975)
- 26 A.B. Wittkower, H.D. Betz: *At. Data* **5**, 113 (1973)
- 27 K. Shima, T. Ishihara, T. Mikumo: *Nucl. Instrum. Methods* **200**, 605 (1982)